The University of Akron

IdeaExchange@UAkron

Chemical and Biomolecular Engineering Faculty Research

Chemical and Biomolecular Engineering Department

7-1-2005

Spm Oxidation and Parallel Writing on Zirconium Nitride Thin Films

N. Farkas

J. R. Comer

G. Zhang

Edward A. Evans
University of Akron Main Campus, evanse@uakron.edu

R. D. Ramsier

See next page for additional authors

Please take a moment to share how this work helps you through this survey. Your feedback will be important as we plan further development of our repository.
Follow this and additional works at: http://ideaexchange.uakron.edu/chemengin_ideas

Part of the Chemistry Commons

Authors

N. Farkas, J. R. Comer, G. Zhang, Edward A. Evans, R. D. Ramsier, and J. A. Dagata

SPM oxidation and parallel writing on zirconium nitride thin films

N. Farkas, J. R. Comer, G. Zhang, E. A. Evans, and R. D. Ramsier[a]
Departments of Physics, Chemistry, and Chemical Engineering, The University of Akron, Akron, Ohio 44325

J. A. Dagata
Precision Engineering Division, National Institute of Standards and Technology, Gaithersburg, Maryland 20899-8212

Systematic investigation of the SPM oxidation process of sputter-deposited ZrN thin films is reported. During the intrinsic part of the oxidation, the density of the oxide increases until the total oxide thickness is approximately twice the feature height. Further oxide growth is sustainable as the system undergoes plastic flow followed by delamination from the ZrN–silicon interface keeping the oxide density constant. ZrN exhibits superdiffusive oxidation kinetics in these single tip SPM studies. We extend this work to the fabrication of parallel oxide patterns 70 nm in height covering areas in the square centimeter range. This simple, quick, and well-controlled parallel nanolithographic technique has great potential for biomedical template fabrication. © *2005 American Vacuum Society.* [DOI: 10.1116/1.1864052]

I. INTRODUCTION

This paper extends our previous studies on SPM oxidation of Group IV metals and their nitrides[1–3] with primary emphasis on ZrN sputtered at high nitrogen flow rates. Our efforts contribute to existing SPM oxidation models[4–12] and provide experimental data for ongoing modeling efforts.[13] Although the overall governing mechanism and the space charge limited oxidation rate is similar for a wide range of materials, we demonstrate that changing the structural and electrical properties of the substrate can significantly alter the oxide growth kinetics. We propose an explanation of the enhanced oxidation and the lack of self-limiting behavior on ZrN surfaces. Successive long time oxidation and etching experiments reveal how the oxide features can grow an order of magnitude higher than the thickness of the film in a sustainable and controllable way.

Transition metal, metal oxide, and metal nitride materials have been extensively used in nanoelectronic device and biocompatible implant production where surface modification is essential to achieve optimal performance. Thus, there is an immense interest in nanoimprint technology[14–19] that provides faster and less expensive pattern transfer than traditional photolithography. In addition to chemical properties, the surface topography of bio-implants plays a critical role in bacteria and cell adhesion.[20,21] Single tip SPM oxidation is an acceptable technique in the field of microelectronics, but it is not efficient for fabricating biomedical templates with large structured areas. However, it is desirable to develop a surface patterning technique for metals that has the inherent simplicity of SPM oxidation. In our efforts to achieve pattern transfer onto ZrN by parallel writing, reported first on silicon by Cavallini *et al.*,[18] detailed understanding of single tip SPM oxidation is necessary. Finding the correct parameters and conditions for the pattern transfer is challenging due to the reactivity of the ZrN. We can now generate robust parallel oxide features 70 nanometers high, attributed to the superdiffusive nature of the ZrN system. The ability to pattern ZrN surfaces across large areas with well-controlled structures of sizes comparable to that of a bacterium provides us with a powerful tool for future bacterial growth studies.

II. EXPERIMENTAL METHODS

The thin films are deposited on boron doped *p*-type Si(111) and Si(100) wafers. Each substrate is ultrasonically cleaned in acetone and isopropanol for 10 min successively. Radio frequency magnetron sputtering is performed at a power of 120 W with a constant argon flow rate of 2 sccm. The nitrogen flow rate is varied from 0 to 10 sccm (total pressure 0.34 – 0.64 Pa) in order to change the stoichiometry of the ZrN films. The substrate holder, positioned 8 cm above the sputtering source, is earthed and there is no temperature control during deposition. The purity of the Zr target is 99.2% (Target Materials, Inc.). Prior to deposition, the system is evacuated to 6×10^{-4} Pa using a turbomolecular pump. The target is sputter-cleaned for 20 min in argon (5 sccm, 55 W) to remove surface oxides and pre-sputtered for 5 min with the same $(Ar+N_2)$ gas mixture used during deposition to stabilize the sputtering conditions. The resulting film thickness is measured with a quartz crystal microbalance.

SPM oxidation is performed under ambient conditions at the National Institute for Standards and Technology (NIST) with a TopoMetrix Accurex II operating in contact mode with uncoated silicon cantilevers from Silicon-MDT Ltd. (Disclaimer: Certain commercial equipment is identified in this article in order to describe the experimental procedure adequately. Such description does not imply recommendation or endorsement by NIST, nor does it imply that the equipment identified is necessarily the best available for the

---

[a]Author to whom correspondence should be addressed; electronic mail: rex@uakron.edu
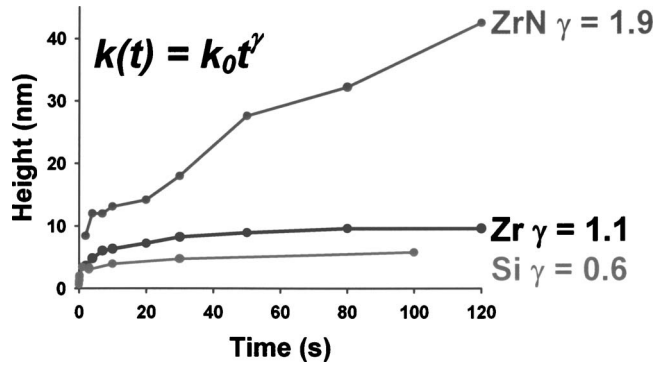
FIG. 1. Comparison of the time dependence of the height of oxide features formed on silicon, zirconium and ZrN (6 sccm). In the time dependent rate constant, $\gamma=1$, $\gamma<1$, and $\gamma>1$ correspond to Brownian-, sub-, and super-diffusion, respectively. Note that the oxide feature height self-limits on silicon and Zr, but not on ZrN.
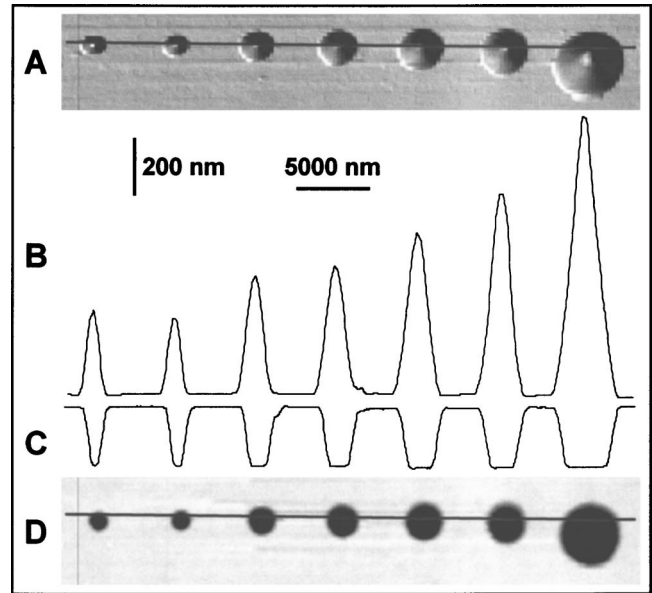

FIG. 2. SPM images (A) and matching cross sections (B) of the oxide features formed on 200 nm thick ZrN sputtered with 5 sccm nitrogen flow rate. 70 V dc voltage is applied for 7, 10, 20, 30, 50, 80, and 120 s, from left to right. (C) and (D) depict the same features after HF etching. Note that the features are much higher, at longer oxidation times, than the thickness of the film.

purpose.) The applied dc voltage varies between 10 and 70 V for various exposure times while the relative humidity is in the range 30%–35%. Given that the Zr and ZrN systems getter considerable amounts of oxygen, thus providing an additional source of oxyanions in addition to ambient water, the oxidation process does not require a glove box to maintain high relative humidity. A negative voltage is applied to the tip with respect to the sample for a fixed amount of time then the tip is moved to another location and the process repeated, so that we produce arrays of features. The anodization time, applied dc voltage, and tip positioning are all computer controlled. The height and width data are extracted from images of the features acquired in contact mode with the same tips used for oxidation. The crystal structure, resistivity and composition of the films are obtained by x-ray diffraction (XRD), four-point probe, and Auger measurements, respectively.

III. RESULTS AND DISCUSSION

XRD and four-point probe measurements[22] reveal that changes in the nitrogen content of the deposition plasma result in significant variations in the structure and resistivity of the films, respectively. As the nitrogen content of the sputtering plasma increases, the structural disorder of the films also increases. Gold colored films obtained with a 0.5 sccm nitrogen flow rate correspond to the stoichiometric ZrN. Below this flow rate the films appear metallic and become increasingly dielectric at higher flow rates. These transitions are consistently reflected in the SPM oxidation kinetics. Higher oxide features are formed at longer exposure times on ZrN substrates prepared with higher nitrogen flow rates. In this regime the deposition rate is low, the resistivity is large and the films are amorphous. Films deposited with 0.5 or lower sccm nitrogen flow rate exhibit self-limited oxidation, while there is no sign of self-limited growth above this value.

Figure 1 compares the time dependence of oxide feature heights formed on silicon, zirconium metal, and zirconium nitride sputtered with a 6 sccm nitrogen flow rate. The γ values from the time-dependent rate constant $k=k_0t^{\gamma}$ show

that silicon is subdiffusive ($\gamma<1$) while the ZrN system exhibits superdiffusive ($\gamma>1$) kinetics.[13] The oxide feature height self-limits around a few tens of nanometers on silicon whereas heights of several hundred nanometers can be obtained in a controllable way on ZrN prepared with higher nitrogen flow rates.

Figures 2(A) and 2(B) show typical SPM images and the corresponding cross sections of a time series of oxide features formed on a ZrN film prepared with a 5 sccm nitrogen flow rate. The symmetrical and well-defined shape of the features is an indication of controlled oxidation and minimal tip wear. Cross sections of features grown on a 200 nm ZrN film reveal that they are one to two orders of magnitude larger than found for other material systems and at longer times higher than the thickness of the film itself. This fact raises the following questions: Where does the material come from, how does the density of the oxide compare to the density of the ZrN film, and what happens at the ZrN–silicon interface? To answer these questions we selectively etch the zirconium oxide using dilute 2%–5% HF solution. A resulting SPM image after etching is shown in Fig. 2(D). Cross sections of the etched features show that the oxide reached the silicon interface at longer oxidation times [Fig. 2(C)].

HF etching reveals the oxide volume beneath the surface and thus the amount of ZrN consumed. Combining these data with the oxide volume above the surface allows us to then calculate the density of the oxide. The etching experiments are repeated also on a 400 nm thick ZrN film sputtered with a 5 sccm nitrogen flow rate to investigate the effect of film thickness. Figure 3 shows the apparent density of the oxide as a function of the oxide height for the two different
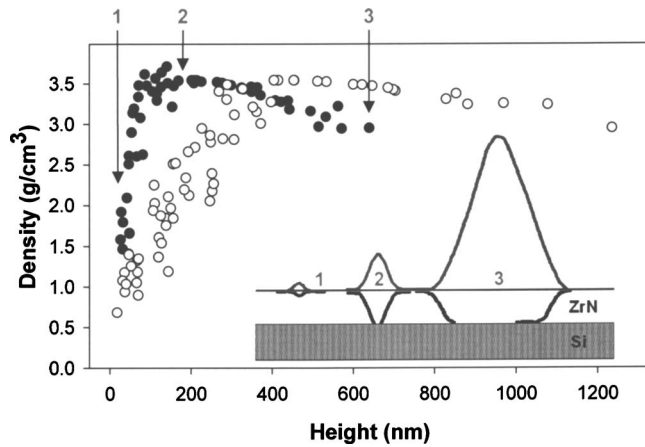
FIG. 3. Apparent density vs oxide height of features generated on 200 nm (filled circles) and 400 nm (unfilled circles) ZrN films. Both films are prepared with a 5 sccm nitrogen flow rate. The inset shows cross sections of features grown on the 200 nm film before and after HF etching.

film thicknesses. The graph indicates that the apparent density starts to decrease roughly at oxide feature heights of 200 and 400 nm—comparable to the thicknesses of the films. The three cross sections in the inset represent the evolution of the apparent density with oxide growth. The density increases until the total oxide volume is approximately twice that of the consumed material and then as the oxidation reaches the ZrN–silicon interface the apparent density begins to decrease as seen in Fig. 3.

To explore the structure of the larger features with lower apparent density, we apply successive voltage pulses until the features crack and eventually split open due to the built-up stress. This sequence is illustrated by the consecutive SPM images and matching cross sections shown in Figs. 4(A)–4(E). Scanning electron microscopy (SEM) and optical images (Fig. 5) of the feature depicted in Fig. 4(E) reveal that it is an oxide shell. The top part which landed upside down provides information about the inside texture of the oxide, as shown in Fig. 5(B). These images of oxide shells allow us to calculate their actual density. We find that the actual oxide volume is approximately twice the volume of ZrN consumed during the SPM oxidation. As the oxidation reaches the ZrN–silicon interface delamination occurs. The apparent density decrease in Fig. 3 is a clear indication of delamination and also shows that the film thickness and the beginning of the delamination are closely related.

Better understanding of the local oxidation of the ZrN system provides a starting point to use the superdiffusive kinetics for future applications. A previous method reported by Cavallini *et al.*[18] and Yokoo[19] extended SPM single tip oxidation to parallel writing. Similar to SPM oxidation, as a voltage is applied between a stamp and a substrate in the presence of water vapor, the high electric field generates oxyanions and initiates oxide growth. This method allows pattern transfer on the square centimeter scale. The obtained feature heights are only a few nanometers on subdiffusive silicon.[18,19] Above we have demonstrated that single tip SPM oxide feature heights formed on superdiffusive ZrN are sig-
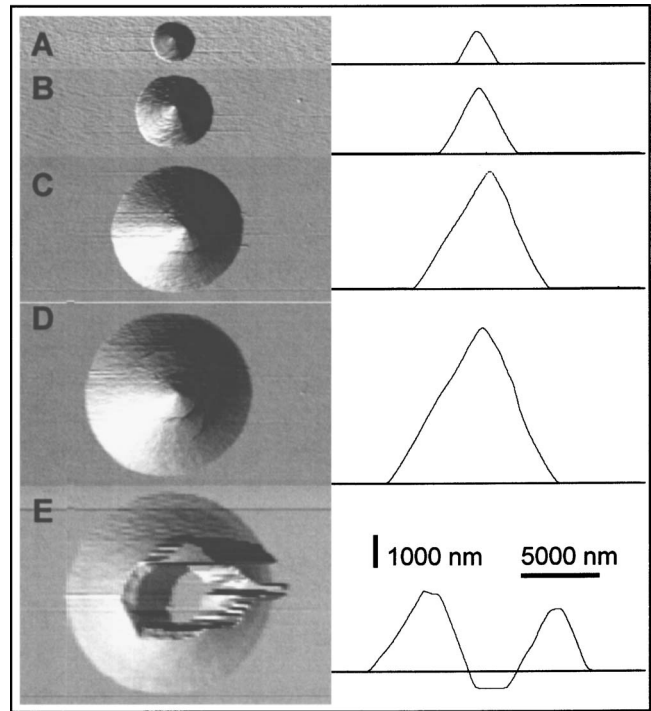

FIG. 4. SPM images and corresponding cross sections of oxide features formed on ZrN sputtered with 2.5 sccm nitrogen flow rate. 70 V is consecutively applied for (A) 2, (B) 14, (C) 44, (D) 76, and (E) 153 min. Concentric cracks develop on the features as seen in (C) and (D), before it splits open as seen in (E).

nificantly larger than for silicon. Below we demonstrate that this enhanced oxide growth can be successfully used to generate 70 nm high oxide features in 20 s exposure time using a parallel writing scheme on ZrN surfaces.

To extend the parallel writing technique to ZrN we use PdAu coated silicon stamps fabricated by standard photolithography at NIST.[23] The 1 cm×4 cm stamp consists of dif-
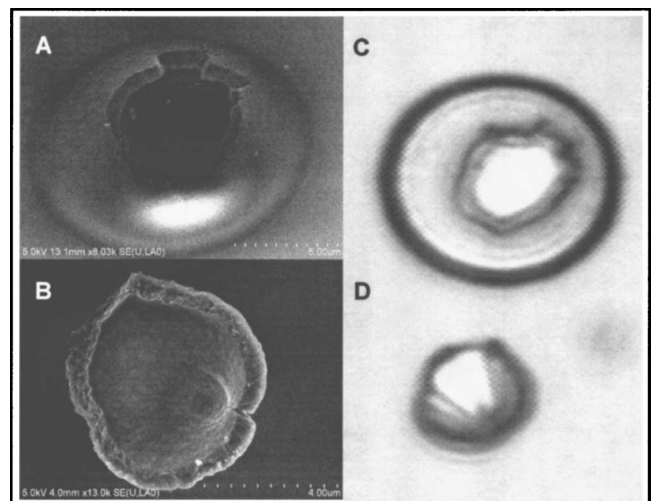

FIG. 5. (A) SEM (Hitachi S-4700) and (C) optical (500X) images of the feature shown in Fig. 4(E). The top part of the feature seen in (B) and (D) landed upside down as the shell cracked open. The SEM image (B) provides information about the inside texture and thickness of the oxide shell.
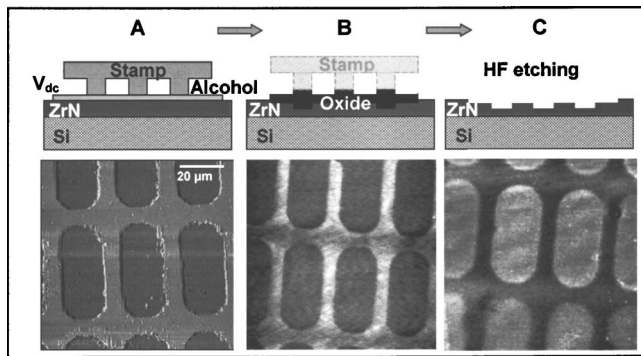
FIG. 6. SPM images of (A) a portion of the PdAu coated silicon stamp, (B) the corresponding oxide pattern transferred onto ZrN, and (C) the pattern after HF etching. The top part of the figure presents a schematic of the main parallel oxidation steps.

ferent sized and shaped isoareal geometrical features 730 nm in height. The top portion of Fig. 6 shows a schematic representation of the main steps of parallel writing on ZrN. As there is a significant difference in the SPM oxidation of ZrN and silicon, the parallel writing technique has to be adapted accordingly. In the case of silicon, water plays an important role as the source of oxyanions. Using water for pattern transfer to ZrN causes considerable damage to the entire film. Given that the ZrN films getter considerable amounts of oxygen, water can be replaced by less-reactive isopropyl alcohol. Higher applied dc voltages of 70–300 V are required for pattern transfer on ZrN in good agreement with the single tip SPM oxidation.

Figures 6(A) and 6(B) present SPM images of a silicon stamp and the matching oxide pattern formed on a ZrN film. Auger analysis[24] of the treated area verifies that oxidation occurs during pattern transfer and confirms that nitrogen is replaced by oxygen. Nitrogen–oxygen replacement has also been reported on TiN and Si_3N_4 substrates.[25,26] In the same way as the oxide is removed after SPM oxidation, we can etch away the parallel oxide pattern using dilute 2%–5% HF solution with good selectivity with respect to ZrN. The SPM image following etching shown in Fig. 6(C) is reversed because oxidation, and therefore, etching occurs below the surface. Cross-section analyses of the parallel oxide patterns before and after HF etching reveal 70 nm oxide heights and that the total thickness of the oxide is about twice the oxide height, similar to the single tip experiments.

IV. SUMMARY STATEMENTS

Oxidation kinetics and material characterization studies of ZrN thin films provide a comprehensive understanding of single tip oxidation and allow us to compare it to that of subdiffusive silicon. The electric field creates the available oxyanions in the very early period of the oxidation. In addition to their direct conversion into oxide, indirect transport of the oxyanions through trap sites also results in oxide formation.[9] In the case of subdiffusive silicon the indirect

transport of oxyanions is hindered by the space charge build-up. Consequently not all of the available reactants convert into oxide resulting in self-limiting behavior.

In the ZrN system the space charge build-up can be suppressed as nitrogen replaced by oxygen reacts with hydrogen and leaves the reaction zone. Moreover, the ZrN systems are capable of forming channels in the oxide network promoting the indirect oxyanion transport. Therefore, the oxidation goes to completion. During this intrinsic oxide formation the density of the zirconium oxide increases until the total oxide volume is roughly twice that of the consumed ZrN. The ZrN films getter significant amounts of oxygen providing additional oxyanions which make further growth possible in the plastic flow regime. With increasing exposure time, the oxidation reaches the ZrN–silicon interface. Delamination occurs when the height of the features reaches the thickness of the film, and with further growth the thickness of the oxide shell remains the same and only the delamination area increases which keeps the oxide density constant.[27] Concentric cracks develop on the delaminated features until they split open.

The nitrogen content of the deposition plasma alters not only the electrical and structural properties of the ZrN films but the network forming ability for oxide formation. More significantly, the competitive outcome of these changes is a continuous variation of γ that reflects the superdiffusivity of the system as the nitrogen content of the sputtering plasma increases.[13] Since parallel writing is governed by the same principles as SPM single tip oxidation, the two techniques exhibit similarities. For instance, in both cases nitrogen is replaced by oxygen and the resulting oxide can be etched away in dilute HF solution with good selectivity. The height of SPM and parallel oxide features on superdiffusive ZrN surfaces is significantly larger than on subdiffusive silicon.

[1]N. Farkas, J. C. Tokash, G. Zhang, E. A. Evans, R. D. Ramsier, and J. A. Dagata, J. Vac. Sci. Technol. A **22**, 1879 (2004).
[2]N. Farkas, G. Zhang, K. M. Donnelly, E. A. Evans, R. D. Ramsier, and J. A. Dagata, Thin Solid Films **447-448**, 468 (2004).
[3]N. Farkas, G. Zhang, E. A. Evans, R. D. Ramsier, and J. A. Dagata, J. Vac. Sci. Technol. A **21**, 1188 (2003).
[4]R. Garcia, M. Calleja, and H. Rohrer, J. Appl. Phys. **86**, 1898 (1999).
[5]E. S. Snow, G. G. Jernigan, and P. M. Campbell, Appl. Phys. Lett. **76**, 1782 (2000).
[6]J. A. Dagata, T. Inoue, J. Itoh, K. Matsumoto, and H. Yokoyama, J. Appl. Phys. **84**, 6891 (1998).
[7]E. Dubois and J-L. Bubendorff, J. Appl. Phys. **87**, 8148 (2000).
[8]P. Avouris, T. Hertel, and R. Martel, Appl. Phys. Lett. **71**, 285 (1997).
[9]J. A. Dagata, F. Perez-Murano, G. Abadal, K. Morimoto, T. Inoue, J. Itoh, and H. Yokoyama, Appl. Phys. Lett. **76**, 2710 (2000).
[10]D. Stiévenard, P. A. Fontaine, and E. Dubois, Appl. Phys. Lett. **70**, 3272 (1997).
[11]J. A. Dagata, F. Perez-Murano, C. Martin, H. Kuramochi, and H.

Yokoyama, J. Appl. Phys. **96**, 2386 (2004).

[12]J. A. Dagata, F. Perez-Murano, C. Martin, H. Kuramochi, and H. Yokoyama, J. Appl. Phys. **96**, 2393 (2004).

[13]J. A. Dagata, J. R. Comer, N. Farkas, G. Zhang, E. A. Evans, R. D. Ramsier, J. Appl. Phys. (to be published).

[14]S. Y. Chou, P. R. Krauss, and P. J. Renstrom, Appl. Phys. Lett. **67**, 3114 (1995).

[15]S. W. Pang, T. Tamamura, M. Nakao, A. Ozawa, and H. Masuda, J. Vac. Sci. Technol. B **16**, 1145 (1998).

[16]A. Kumar, H. Biebuyck, and G. M. Whitesides, Langmuir **10**, 1498 (1994).

[17]S. Hoeppener, R. Maoz, and J. Sagiv, Nano Lett. **3**, 761 (2003).

[18]M. Cavallini, P. Mei, F. Biscarini, and R. Garcia, Appl. Phys. Lett. **83**, 5286 (2003).

[19]A. Yokoo, J. Vac. Sci. Technol. B **21**, 2966 (2003).

[20]C. Galli, M. Collaud Coen, R. Hauert, V. L. Katanaev, P. Groning, and L. Schlapbach, Colloids Surf., B **26**, 255 (2002).

[21]B. W. Buczynski, M. M. Kory, R. P. Steiner, T. A. Kittinger, and R. D. Ramsier, Colloids Surf., B **30**, 167 (2003).

[22]G. Zhang, N. Farkas, R. D. Ramsier, E. A. Evans, and J. A. Dagata, Thin Solid Films (to be published).

[23]J. A. Dagata and J. S. Suehle (unpublished).

[24]N. Farkas, J. R. Comer, G. Zhang, E. A. Evans, R. D. Ramsier, S. Wight, and J. A. Dagata, Appl. Phys. Lett. **85**, 5691 (2004).

[25]S. Gwo, C.-L. Yeh, P.-F. Chen, Y.-C. Chou, T. T. Chen, T.-S. Chao, S. F. Hu, and T.-Y. Huang, Appl. Phys. Lett. **74**, 1090 (1999).

[26]F. S.-S. Chien, Y.-C. Chou, T. T. Chen, W.-F. Hsieh, T.-S. Chao, and S. Gwo, J. Appl. Phys. **89**, 2465 (2001).

[27]N. Farkas, J. R. Comer, G. Zhang, E. A. Evans, R. D. Ramsier, J. A. Dagata, Nanotechnology **16**, 262 (2005).